

# Dynamic mechanical, mechanical and thermal analysis of CPI/NBR blends: effect of blend composition and crosslink density

Mahesh Baboo<sup>1</sup> · Seema Gupta<sup>1</sup> · Kananbala Sharma<sup>1</sup> · N. S. Saxena<sup>1</sup>

Received: 20 June 2015 / Accepted: 19 December 2015 / Published online: 30 December 2015  
© Springer-Verlag Berlin Heidelberg 2015

**Abstract** Blends of *cis*-polyisoprene (CPI) and nitrile butadiene rubber (NBR) in different volume ratio were prepared to see the effect of composition on different properties. Structure characterization has been done through X-ray diffraction and scanning electron microscope. Scanning electron micrographs confirm homogeneous nature of all the blends. The dynamic mechanical analyzer was used to measure damping, storage modulus, glass transition temperature and mechanical properties (Young's modulus and tensile strength) of these blends. Activation energy and fragility were determined for the non-Arrhenius (fragile) behavior of viscosity using Vogel–Fulchuer–Tammann (VFT) equation. Thermal conductivity has been analyzed through thermal constant analyzer. Results indicate that all the measured properties are dependent on blend composition and crosslink density.

**Keywords** Thermal properties · Mechanical properties · Glass transition temperature · Activation energy · Fragility

## Introduction

Blending of two or more polymers is a technique which has received increasing attention for the last few decades from the view point of their different physical properties not obtained either by the polymers or their copolymers. *Cis*-polyisoprene (CPI or NR) is a widely used polymer for various products such as tyres, o-rings and gaskets. Also, it has some specific properties different [1, 2] than those of nitrile butadiene rubber (NBR), which is a copolymer of acrylonitrile and butadiene, and offers a very good resistance to hydrocarbon oil [3]. CPI is commercially available

---

✉ Mahesh Baboo  
m.baboo@rediffmail.com

<sup>1</sup> Semiconductor and Polymer Science Lab, Room No. 14-15, Department of Physics, University of Rajasthan, Jaipur 302004, India

at very low cost and is known to have the ability to strain-induced crystallization [1, 2] as compared to NBR. However, it suffers from poor resistance [1, 2] to chemicals and oil. Thus, the uses of any one of these in commercial applications are limited.

Therefore, blends of CPI with NBR are the mixtures of interest to develop a material to find its application in industry. In this direction, Azima et al. [4] have reported compatibility studies on CPI/NBR blends by electrical and mechanical techniques and found that CPI/NBR blends were immiscible. Sirisinha et al. [5] studied chemical and mechanical properties and found that blend morphology has an impact on both the properties. It was also reported [4, 6] that blending of NBR with CPI produces oil-resistant compound with good tensile strength. More recently, Kumari et al. [7] have reported the effects of the blend ratio, compatibilizer, penetrant size, and temperature on the vapor permeability of CPI/NBR blend membranes. The influence of blend ratio, crosslinking systems, fillers and compatibilizer on morphology and thermal stability of different CPI/NBR blends has also been investigated by Kumari et al. [8] in another study and the results showed that (1) the thermodynamic immiscibility of the CPI/NBR blends and (2) thermal stability increase with increasing NBR concentration in the blends.

Among the various properties, dynamic mechanical, mechanical and thermal properties of polymers have much interest due to remarkable modifications observed after blending [9–11]. These properties play an important role in deciding a material to find application in required fields [12, 13]. Therefore, knowledge of these properties is essential. Although, there are many dynamic mechanical and mechanical parameters which decide the overall load-bearing performance of a polymer but few of them such as storage modulus,  $\tan \delta$ , glass transition, tensile strength and Young's modulus [14, 15] are of more importance. In addition to these dynamic mechanical and mechanical parameters, activation energy and fragility are also important parameters [16, 17] to characterize the material. Fragility classifies the material as a strong or fragile liquid. A fragile material shows a very abrupt change in physical properties like storage modulus and viscosity as it approaches  $T_g$ , whereas strong materials show a strong resistance to change in properties with temperature, undergoing a relatively smooth transition from the glassy state to rubbery state. Therefore, fragility of a material is a measure of structural stability [16, 17]. Activation energy for glass transition of a polymer represents the potential energy barrier that the motion of the chain segments has to overcome for the transition to occur [18]. Information regarding the thermal properties of polymer blends is required in the efficient and economical design of all process operations involving heat transfer as the proper control or optimization of such process depends largely on heat transfer [19, 20]. Problems of heat removal in processes involving microelectronics, thermally conductive adhesives and the power generation industries, material are chosen primarily considering their thermal properties [21]. In case of blends, dynamic mechanical, mechanical and thermal properties are dependent on properties of its constituents, morphology, interphase adhesion, crystallinity, molecular weight and crosslink density of final material [22, 23].

Thus, a plethora of work has been done on strain-induced crystallization, crosslinking, thermodynamic compatibility, resistance to hydrocarbon oil and tensile strength of CPI/NBR blends but very little efforts have been made to study

the thermal and thermo-mechanical properties of these blends. Present paper reports the effect of blend ratio on storage modulus, glass transition temperature, activation energy, fragility, mechanical properties and thermal conductivity. Besides, an effort has also been made to establish a correlation between crosslink density and measured properties.

## Experimental

### Materials

Acrylonitrile butadiene rubber (NBR) with 18 % acrylonitrile content was supplied from Lansex. *Cis*-polyisoprene (CPI) with 97 % *cis*-1, 4 content was purchased from Sigma-Aldrich. Both the materials are in rubbery lump form. Tetrahydrofuran (THF  $\geq 99$  %) were purchased from Merck.

### Preparation of samples

Both CPI and NBR of known polymer compositions were separately dissolved in THF and then mixed in the CPI/NBR volume ratio of 100/0, 75/25, 50/50, 25/75 and 0/100. The solutions were slowly cast on Petri dish and kept for drying in air for a period of 2–3 weeks. To ensure that the sample did not contain solvent, the films were further dried in vacuum for 2 days at ambient temperature. Films were prepared with an average thickness of approximately 1.34 mm for all blends. Uniformity of the thickness of the film has been ensured by measuring the same at different points of the film.

### Characterization

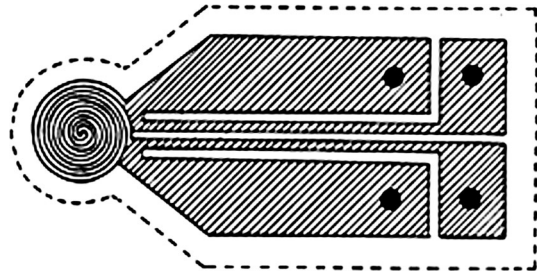
Wide-Angle X-ray Scattering (WAXS) measurements were carried out on a PAnalytical X' pert Pro X-ray diffractometer using copper target (Cu,  $K_{\alpha}$ ) at scanning rate of 3° per minute between 10° and 60°. All the data were recorded in reflection mode.

Morphological analysis has been done using Scanning Electron microscope (Carlzeiss Evo18). Gold coating was applied prior to the recording of images.

Mechanical properties have been measured using Dynamic Mechanical Analyzer (DMA). In this technique, a sinusoidal force is applied to the sample and the amplitude and phase of the resulting displacement are measured. The details of the technique have been discussed elsewhere [24]. For DMA measurements, film samples were cut according to the requirement of the technique and were mounted in single-cantilever bending mode for temperature scan while for stress–strain measurements, samples were mounted in tension mode.

Thermal conductivity ( $\lambda$ ) has been determined using thermal constant analyzer (TCA) which is based on Transient Plane Source (TPS) method [25]. In this method, the transient plane source element (sensor) behaves both as temperature sensor and heat source. TPS sensor (Fig. 1) consists of an electrical conducting pattern of thin

**Fig. 1** Schematic diagram of TPS sensor



nickel foil (10  $\mu\text{m}$ ) in the form of double spiral embedded in an insulating layer made of kapton (70  $\mu\text{m}$ ). Sensor is sandwiched between the two pieces of the samples having perfectly smooth surface so as to ensure perfect thermal contact. Details of TPS technique have been given elsewhere [26].

## Theory

### Determination of crosslink density

Crosslink density is an extremely important factor in rubber-like materials in determining their physical properties. Crosslink density of pure CPI, pure NBR and their blends can be estimated through mechanical method involving stress–strain measurements. The Mooney–Rilvin equation is widely used for assessing crosslink density of rubbers based on their stress–strain behavior. The Mooney–Rilvin equation can be applied to both unswollen and swollen rubbers. For unswollen rubbers, such equations are based on the phenomenological theory of rubber elasticity [27, 28] which can be obtained as follows.

$$\sigma/(\alpha - \alpha^{-2}) = \rho RT \quad (1)$$

where  $\rho$  is the crosslink density,  $\sigma$  is the stress in Pa,  $R$  is the gas constant (8.314 J/mole K),  $T$  is the temperature in K, and  $\alpha$  is the extension ratio  $L/L_0$ . The strain is  $(L - L_0)/L_0$ .

### Determination of activation energy and fragility

Both activation energy ( $E_a$ ) and fragility ( $K$ ) can be determined for the non-Arrhenius (fragile) behavior of viscosity using Vogel–Fulchuer–Tammann (VFT) equation [29]:

$$\eta = \eta_o \exp [1/K\{(T/T_o) - 1\}] \quad (2)$$

and

$$K = E_a/2.303RT_g \quad (3)$$

where  $T_0$  is defined as the VFT temperature, which is roughly 50 °C below the glass transition.

Temperature ( $T_g$ ): This is the temperature at which viscosity ( $\eta$ ) also reaches its maximum value. Temperature dependence of viscosity has been obtained from the temperature dependence of storage modulus and loss modulus which have been measured using DMA.

Using the value of  $K$  from Eq. (3), Eq. (2) becomes

$$\eta = \eta_0 \exp \left[ \frac{2.303RT_g T_0}{E_a(T - T_0)} \right]. \quad (4)$$

The apparent activation energy ( $E_a$ ) has been obtained from the slop of the linear fit of the curve [Eq. (4)] between  $\log \eta$  and  $1/\{(T/T_0) - 1\}$  while fragility ( $K$ ) has been calculated using Eq. (3).

### Determination of thermal conductivity

For the measurement of thermal conductivity of thin film with thickness of the order of microns, the experiment was performed in two steps. In the first step, sensor is sandwiched between the two pieces of the sample—each with a plane surface facing the sensor. This arrangement was placed between the two auxiliary metal (stainless steel) pieces as shown in the Fig. 2.

Data for the temperature increase over a given time were collected using the software available with the Hot Disk Thermal Constant Analyzer TPS (model 2500S). In the second step, the experiment was repeated with the Hot Disk sensor sandwiched between the same two pieces of the metal and data for the temperature increase were again collected taking the same experimental conditions as mentioned above.

Employing these two temperature increases (Fig. 3), thickness of the film and power delivered to the sample, the thermal conductivity of thin film sample can be determined through the following relation:

$$\lambda = (P \cdot \Delta x) / (2A \cdot \Delta T) \quad (5)$$

where  $P$  is the total output power given to the sensor,  $A$  is the area of conducting pattern of sensor,  $\Delta x$  is the thickness of thin samples and  $\Delta T$  is the temperature difference across the samples.

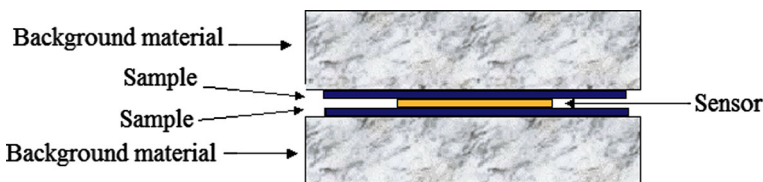


**Fig. 2** Illustration for the measurement of thermal conductivity of thin film

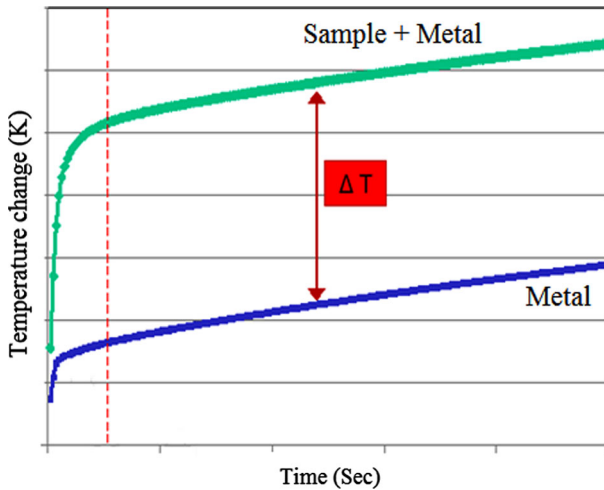


**Fig. 3** Temperature difference across the sample with background material

## Result and discussion

### Structural characterization

#### *X-ray diffraction*

Figure 4 shows the XRD patterns for different CPI/NBR blends. The diffraction patterns of all the blends show a broad hallow at  $2\theta = 20^\circ$  which is the signature of the amorphous nature of the samples. However, intensity of hallow increases with increasing concentration of NBR in the CPI/NBR blend and it is highest for pure NBR. Thus, NBR is less amorphous material as compared to CPI.

#### *Morphology*

Scanning electron micrographs of pure CPI, pure NBR and their two (25/75 and 75/25) blends as representative cases are depicted in Fig. 5 which represents the morphology of the samples. From Fig. 5a and b, it is clear that phase separation is not present in both the blends. However, sample CPI-25/NBR-75 seems to more compatible morphology than sample CPI-75/NBR-25 as also exhibited by mechanical and thermal properties of these blends. Although CPI/NBR blends have multi-phase morphology [4, 5, 30] but here NBR has low acrylonitrile content with nearly similar viscosity to CPI which might be responsible for compatibility [31] of both the materials. Thus, morphology studies revealed that CPI/NBR blends are miscible (homogeneous) which is also confirmed by the dynamic mechanical measurements (glass transition temperature) of this article.

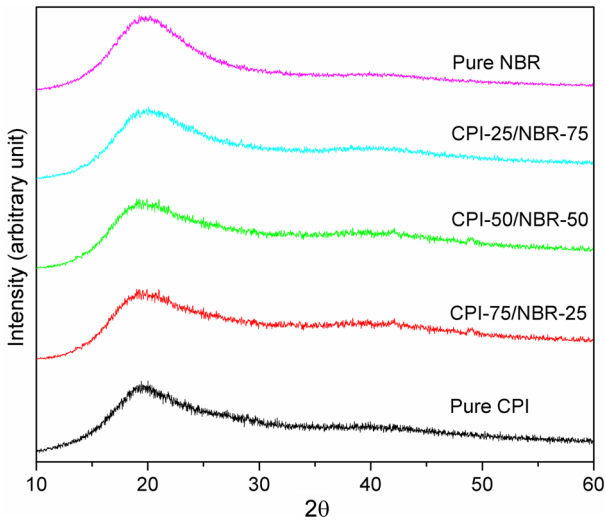


**Fig. 4** X-ray diffraction patterns for different CPI/NBR blends

## Dynamic mechanical properties

### *Glass transition temperature and damping property*

The dependence of  $\tan \delta$  on blend ratio and temperature is illustrated in Fig. 6. The curves of  $\tan \delta$  against temperature show well-defined and symmetric peaks corresponding to the relaxation associated to the transition from glassy state to the elastic state of the blends. The characteristic temperature corresponding to the peak point is identified as glass transition temperature [24]. All the blends show a single peak, indicating a single but separate glass transition temperature, which confirms that the blends are miscible as observed from SEM micrographs. The glass transition temperatures corresponding to peak of  $\tan \delta$  curves of all the samples are given in Table 1. The glass transition temperatures of pure CPI and pure NBR are at  $-46$  and  $-38^\circ\text{C}$ , respectively. Also, there is a slight shifting in the value of  $T_g$  of pure NBR in positive side with increasing NBR concentration in the CPI/NBR blends. However, the values of  $T_g$  for the samples pure NBR and CPI-25/NBR-75 are same. This observed behavior of glass transition temperature can be explained on the basis of crosslink density [32]. When higher crosslinked material is subjected to temperature variation from low to room, the free volume of molecules of chains in the material increases but this increase in free volume will be less than the increase in free volume for a lower crosslinked material to same temperature variation. Therefore, higher energy (higher activation energy is confirmed in further of this article) is required to make a transition from glassy phase to rubbery phase for higher crosslinked materials. As a result  $T_g$  obtained for higher crosslinked material is higher than that observed for lower crosslinked material.

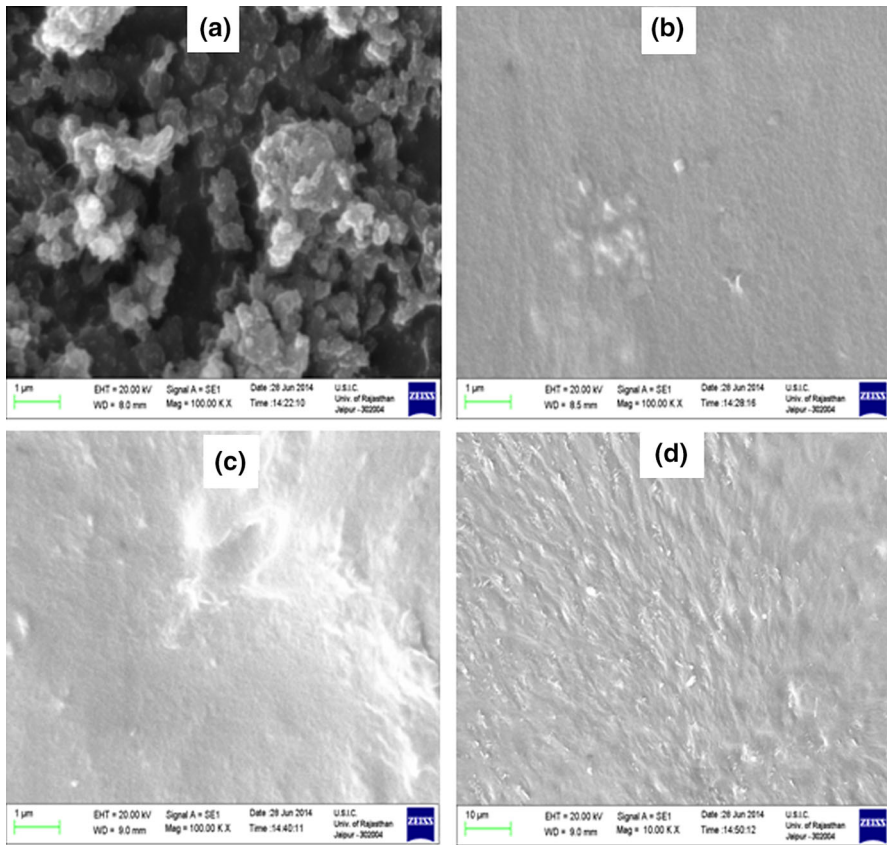


**Fig. 5** SEM micrographs of CPI/NBR blends; **a** pure CPI, **b** CPI-75/NBR-25, **c** CPI-25/NBR-75, **d** pure NBR

The height of  $\tan \delta$  peak in Fig. 6 presents the damping of the materials. From this figure, it is observed that the height of  $\tan \delta$  peak, and in turn damping, is highest for pure CPI and lowest for pure NBR and decreases with increasing NBR concentration in CPI/NBR. However, the blend CPI-50/NBR-50 has nearly same damping at that of pure NBR. It is reported [32] that higher crosslinked materials have higher damping than lower crosslinked materials. So, the observed behavior of damping for all the samples can be explained on the basis of crosslink density calculated by Mooney–Rilvin Equation and given in Table 1.

### *Storage modulus*

The dependence of storage modulus on blend ratio and temperature is shown in Fig. 7. From this figure (inset figure), it is observed that the values of storage modulus in the temperature range  $-40$  to  $20$  °C increase with increasing NBR concentration in the CPI/NBR blends and this behavior of storage modulus is not



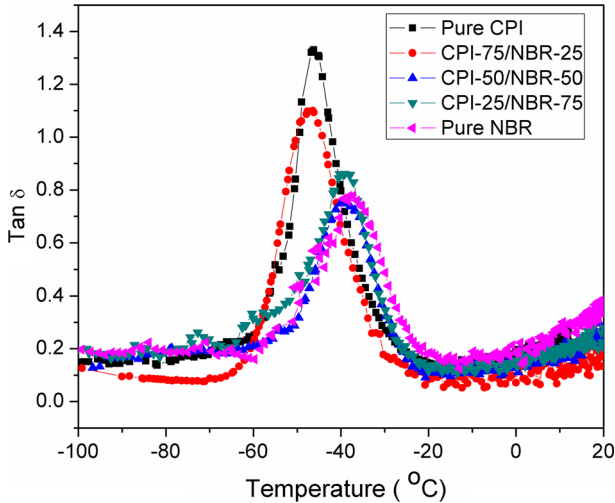


**Fig. 6** Variation of  $\tan \delta$  with temperature for different CPI/NBR blends

**Table 1** Values of glass transition temperature and crosslink density for different CPI/NBR blends

Sample name	Crosslink density (mole/m <sup>3</sup> )	Glass transition temperature (°C)
Pure CPI	30	−38
CPI-75/NBR-25	28	−39
CPI-50/NBR-50	27	−40
CPI-25/NBR-75	23	−46
Pure NBR	22	−46

followed by the sample CPI-75/NBR-25 in the temperature range nearly −40 to −100 °C. This observed behavior of storage modulus can be explained on the basis of crosslink density (Table 1) as higher value of crosslink density reduces the mobility of molecular chain segments which leads to increase in modulus. The higher value of storage modulus observed for sample CPI-75/NBR-25 in the temperature range nearly −40 to −100 °C might be attributed to the different cold crystallization of this sample [32]. Another observation that can be made from the Fig. 7 is that all the samples, excluding sample CPI-75/NBR-25, exhibit second-order [24] transitions ( $\gamma$  and  $\beta$ ) in the temperature range nearly −97 to −42 °C. The same can also be confirmed in  $\tan \delta$  curves. Storage modulus also varies with temperature (Fig. 7): as temperature increases, there is an initial small decline followed by a steep fall before another gradual descent to a constant value. This observed behavior gives support to the ‘crankshaft mechanism’, which gets its name from the chain in the amorphous regions, coordinated large-scale motion, similar to the movement of the crankshaft in an engine, as the temperature rises [24].

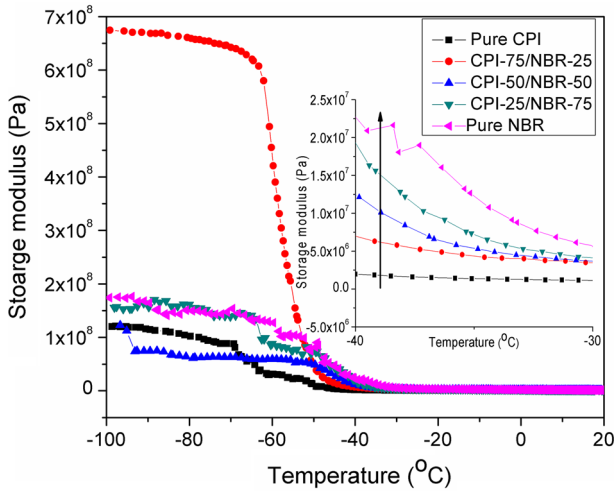


**Fig. 7** Variation of storage modulus with temperature for different CPI/NBR blends

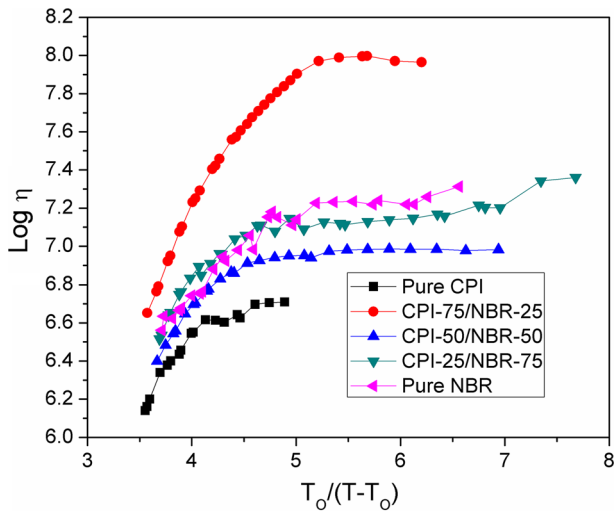


**Fig. 8** Fragility plot for different CPI/NBR blends

*Activation energy and fragility*

Figure 8 represents the fragility plot for different CPI/NBR blends from which activation energy has been determined and depicted in Fig. 9. From Fig. 9, it is observed that activation energy increases with increasing NBR concentration in the CPI/NBR blends. This observed behavior of activation energy is due to the increase in crosslink density by the increase in NBR concentration in CPI/NBR blends. As

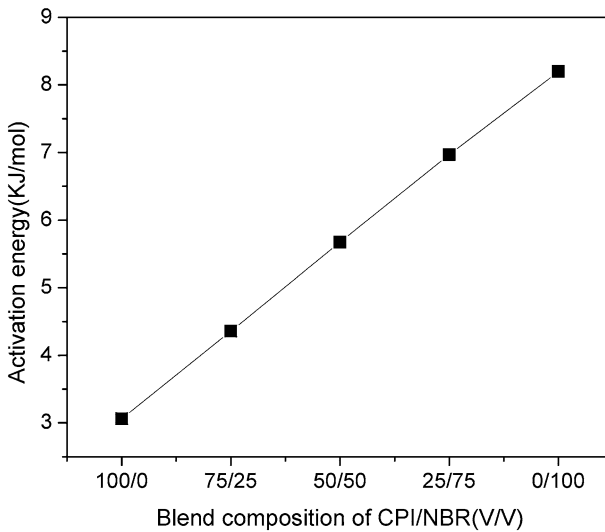


**Fig. 9** Variation of activation energy with blend composition

the motion of molecules in glass transition region is governed by to crosslink density, and increase in crosslink density decreases the free volume as well as oscillations of molecules about mean position. Thus, increase in NBR concentration in CPI/NBR blends reduces the motion of chains and therefore higher energy is required to make molecule mobile.

Figure 10 represents the variation of fragility with blend composition of CPI/NBR. From this figure, it is clear that fragility increases with increasing NBR concentration. This can be explained on the basis of crosslink density. It has been reported [33] that polymers with rather simple, less sterically hindered structure (i.e. lower crosslink density) are usually strong, while polymers with rigid structure (i.e. higher crosslink density) or sterically hindered backbones are usually fragile. Therefore, increase in crosslink density (Table 1) due to increase in NBR concentration increases the fragility.

### Mechanical properties

The stress–strain behavior of a material is extremely helpful to understand the nature of the deformation of the blends under an applied load. The stress–strain curves of pure CPI, pure NBR and their blends are shown in Fig. 11. Deformation curves of all the samples are similar. Mechanical properties such as tensile strength and young's modulus have been determined through these stress–strain curves and given in Figs. 12 and 13. It can be understood from Figs. 12 and 13 that both tensile strength and Young's modulus are lowest for pure CPI while highest for pure NBR and as the concentration of NBR increases in CPI/NBR blend, both the values of tensile strength and Young's modulus also increase. This is due mainly to the crosslink density. The increase of NBR concentration in CPI/NBR blend enhances

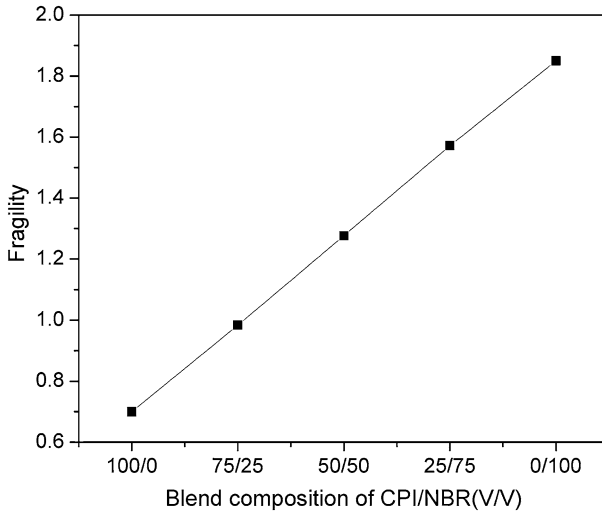


**Fig. 10** Variation of fragility with blend composition

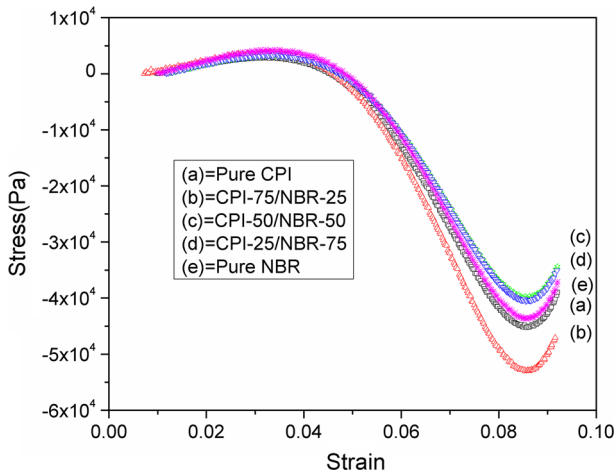


**Fig. 11** Stress–strain curves for different CPI/NBR blends

crosslink density (Table 1) which restricted chain mobility and as a result reduces the ability of the chain to respond to a load or stress to which the sample is subjected [34] and therefore both tensile strength and Young' modulus increase.

### Thermal conductivity

The effect of blend ratio on thermal conductivity is illustrated in Fig. 14. From this figure, it is observed that thermal conductivity of pure CPI is lowest while it is

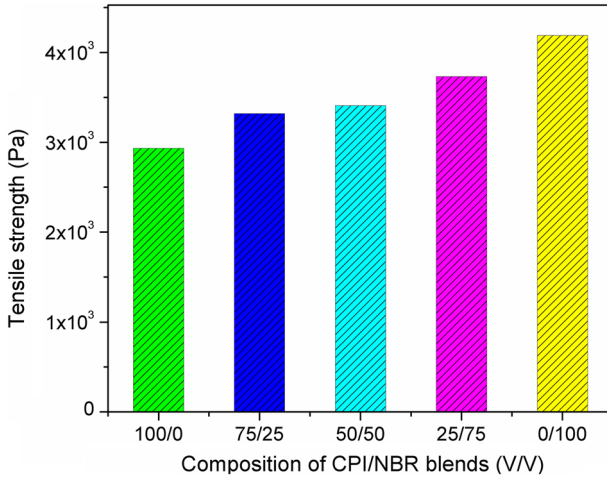


**Fig. 12** Variation of tensile strength with blend composition

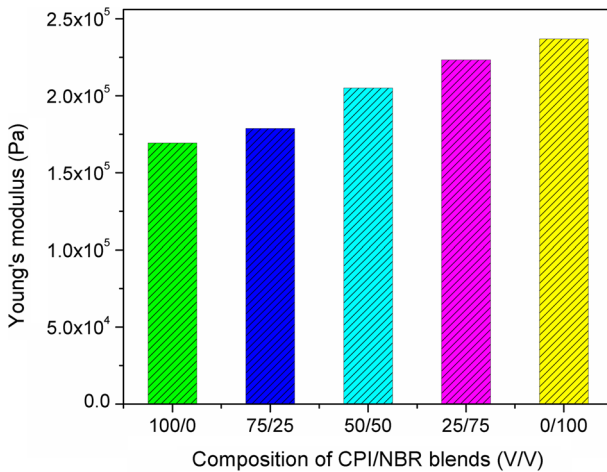


**Fig. 13** Variation of Young's modulus with blend composition

highest for pure NBR and increases with increasing NBR concentration in the CPI/NBR blend. This observed behavior of thermal conductivity of pure CPI, pure NBR and their blends can be explained on the basis of crystallinity and crosslink density. It has been reported [35] that thermal conductivity of a material is associated with its crystallinity and crosslink density, and increases with increasing crystallinity and crosslink density of the material. As pure CPI is more amorphous (Fig. 1) as compared to pure NBR; therefore, thermal conductivity of pure CPI is lower than pure NBR. Also, lower crosslink density (Table 1) of pure CPI than pure NBR is responsible for lower thermal conductivity of pure CPI than pure NBR. In case of

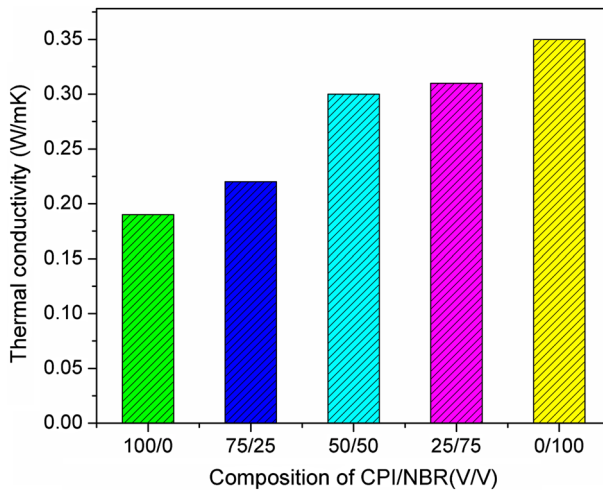


**Fig. 14** Variation of thermal conductivity with blend composition

blends, as the concentration of NBR in CPI/NBR blend increases, crosslink density of the material increases (Table 1) and as a result thermal conductivity also increases.

## Conclusions

X-ray measurements confirm that CPI, NBR and their blends are amorphous materials. SEM analysis suggests that all the blends of CPI/NBR are homogeneous. Dynamic mechanical, mechanical and thermal analyses reveal that blends of CPI/NBR present additive behavior for all the determined properties. Also, crosslink density of the blends increases with NBR concentration and showing an impact on all the determined properties.

**Acknowledgments** The work was supported by Science and Engineering Research Board (SERB, DST), New Delhi (Grant No. SR/FTP/PS-146/2011) under FAST TRACK Scheme for Young Scientist.

## References

1. Kantala C, Wimolmala E, Sirisinha C, Sombatsompop N (2009) Reinforcement of compatibilized NR/NBR blends by fly ash particles and precipitated silica. *Polym Adv Technol* 20:448–458
2. Moonprasith N, Suchiva K, Tongcher O, Blending in latex form of natural rubber and nitrile lattices: a preliminary study of morphology and mechanical properties. <http://www2.mtec.or.th/th/seminar/Msativ/pdf/PP13.pdf>. Accessed 10 June 2015
3. Joseph R, George KE, Francis DJ (1988) Studies on the cure characteristics and vulcanizate properties of 50/50 NR/SBR blend. *J Appl Polym Sci* 35:1003–1017
4. Saad ALG, El-Sabbagh S (2001) Compatibility studies on some polymer blend systems by electrical and mechanical techniques. *J Appl Polym Sci* 79:60–71

5. Sirisinha C, Baulek-Limcharoen S, Thunyarittikorn J (2001) Relationships among blending conditions, size of dispersed phase, and oil resistance in natural rubber and nitrile rubber blends. *J Appl Polym Sci* 82:1232–1237
6. Ismail MN, El-Sabbagh SH, Yehia AA (1999) Fatigue and mechanical properties of NR/SBR and NR/NBR blend vulcanizates. *J Elastomers Plast* 31:255–270
7. Kumari P, Kakkadantavida C, Radhakrishnan Panicker G, Unnikrishnan Varghese S, Sujith A (2010) Natural rubber/acrylonitrile butadiene rubber blend membranes: vapor permeation properties. *Chem Eng Technol* 33:97–102
8. Kumari P, Unnikrishnan G (2013) Thermal properties of compatibilized and filled natural rubber/acrylonitrile butadiene rubber blends. *J Thermal Anal Calor* 114:67–75
9. Shundo M, Imoto M, Minoura Y (1966) Studies on polymer blends: blending methods for natural rubber and styrene rubber. *J Appl Polym Sci* 10:939–953
10. George SC, Ninan KN, Groeninckx G, Thomas S (2000) Styrene-butadiene rubber/natural rubber blends: morphology, transport behavior, and dynamic mechanical and mechanical properties. *J Appl Polym Sci* 78:1280–1303
11. Ismail H, Leong HC (2001) Curing characteristics and mechanical properties of natural rubber/chloroprene rubber and epoxidized natural rubber/chloroprene rubber blends. *Polym Testing* 20:509–516
12. Ramesan MT, Alex R, Khanh NV (2005) Studies on the cure and mechanical properties of blends of natural rubber with dichlorocarbene modified styrene-butadiene rubber and chloroprene rubber. *React Funct Polym* 62:41–50
13. Komalan C, George KE, Kumar PAS, Varughese KT, Thomas S (2007) Dynamic mechanical analysis of binary and ternary polymer blends based on nylon copolymer/EPDM rubber and EPM grafted maleic anhydride compatibilizer. *Express Polym Lett* 1:641–653
14. Baboo M, Dixit M, Sharma KB, Saxena NS (2009) The structure and thermomechanical properties of blends of *trans*-polyisoprene with *Cis*-polyisoprene. *Int J Polym Mater* 58:636–646
15. Baboo M, Dixit M, Sharma KB, Saxena NS (2010) Activation energy and thermo-mechanical properties of *trans*-polyisoprene and liquid *cis*-polyisoprene blends. *Thermochim Acta* 502:47–50
16. Baboo M, Dixit M, Sharma K, Saxena NS (2011) Mechanical and thermal characterization of *cis*-polyisoprene and *trans*-polyisoprene blends. *Polym Bull* 66:661–672
17. Baboo M, Sharma K, Saxena NS (2011) Viscosity, glass transition and activation energy of solid *cis*-polyisoprene and *trans*-polyisoprene blends. *Phase Transit* 84:901–907
18. Manzure A, Sanchez FH (2006) Activation energy for the glass transition of a confined elastomer in HDPE/PP blends. *J Macromol Sci Part B Phys* 45:139–152
19. Najidha S (2007) Structure and properties of polyisoprene modified by chemical and implant doping. Ph.D. Thesis. University of Rajasthan
20. Tavman IH (1996) Thermal and mechanical properties of aluminum powder-filled high-density polyethylene composites. *J Appl Polym Sci* 62:2161–2167
21. Mathur V (2010) Thermal and mechanical study of polystyrene based polymeric blends and their CdS-nanocomposites. Ph.D. Thesis. University of Rajasthan
22. Corish PJ (1978) Science and technology of rubber. Academic Press, New York
23. Fried JR (1999) Polymer science and technology. Prentice Hall of India, New Delhi
24. Menard KP (1999) Dynamic mechanical analysis: a practical introduction. CRC, New York
25. Gustafsson SE (1991) Transient plane source techniques for thermal conductivity and thermal diffusivity measurements of solid materials. *Rev Sci Instrum* 62:797–804
26. Agarwal S, Patidar D, Saxena NS (2013) Effective thermal conductivity of CdS/ZnS nanoparticles embedded polystyrene nanocomposites. *Heat Mass Transf* 49:947–953
27. Sombatsompop N (1998) Practical use of the Mooney-Rilvin equation for determination of degree of crosslinking of swollen NR vulcanisates. *J Sci Soc of Thailand*. 24:199–
28. Gilmer TC, William M (1996) Polymer mechanical properties via a new laboratory tensile tester. *J Chem Educ* 73:1062–1083
29. Sastry S (2001) The relation between fragility, configurational entropy and the potential energy landscape of glass-forming liquids. *Nature* 409:164–167
30. Chokcharoenchai B, Kraitape N, Kattiyabot T, Radsantia R, Thongpin C (2013) Cure characteristics, morphology and mechanical properties of partially cured NBR blended with NR. *Adv Mater Res* 747:463–466
31. Tinker A, Jones KP (1998) Blends of natural rubber: novel techniques for blending with speciality polymers. Springer, Berlin

32. Boochatham P, Chiewnawin S (2001) Vulcanization of *cis*- and *trans*-polyisoprene and their blends: crystallization characteristics and properties. *Eur Polym J* 37:429–434
33. Kumar K, Christopher GR, Pawlus S, Hahn SE, Sokolove AP (2008) Role of chemical structure in fragility of polymers: a qualitative picture. *Macromolecules* 41:7232–7238
34. Shaktawat V, Jain N, Saxena NS, Sharma KB, Sharma TP (2007) Thermomechanical investigation of a thick film of aniline-formaldehyde copolymer and poly(methyl methacrylate). *Polym Sci Series B* 49:236–239
35. Jayasree TK, Predeep P, Agarwal R, Saxena NS (2006) Thermal conductivity and thermal diffusivity of thermoplastic elastomeric blends of styrene butadiene rubber/high density polyethylene: effect of blend ratio and dynamic crosslinking. *Trends Appl Sci Res* 1:278–291